Mass-Dependent and Mass-Independent Isotope Effects of Zinc in a Redox Reaction

ARTICLE *in* THE JOURNAL OF PHYSICAL CHEMISTRY A · OCTOBER 2009

Impact Factor: 2.69 · DOI: 10.1021/jp904882d · Source: PubMed

Mass-Dependent and Mass-Independent Isotope Effects of Zinc in a Redox Reaction

Toshiyuki Fujii,*,† Frédéric Moynier,‡ Akihiro Uehara,† Minori Abe,§ Qing-Zhu Yin,⊥ Takayuki Nagai,# and Hajimu Yamana†

Research Reactor Institute, Kyoto University, 2-1010 Asashiro Nishi, Kumatori, Sennan Osaka 590-0494, Japan, Department of Earth and Planetary Sciences and McDonnell Center for Space Sciences, Washington University in St. Louis, Campus Box 1169, 1 Brookings Drive, Saint Louis, Missouri 63130-4862, Department of Chemistry, Graduate School of Science and Engineering, Tokyo Metropolitan University, 1-1 minami-Osawa, Hachioji-shi, Tokyo 192-0397, Japan, Department of Geology, University of California Davis, One Shields Avenue, Davis, California 95616, and Nuclear Fuel Cycle Engineering Laboratory, Japan Atomic Energy Agency, Tokai, Ibaraki 319-1194, Japan

Received: May 26, 2009; Revised Manuscript Received: August 27, 2009

We report the isotope fractionation of zinc (Zn) associated with a redox reaction between Zn^0 and Zn(II). Zn isotopes were found fractionated in pyrometallurgical biphase extraction between liquid zinc and molten chloride. The isotopic composition of Zn in the molten chloride phase was analyzed by multiple collector inductively coupled plasma mass spectrometry and reported as $^{m}Zn/^{64}Zn$ (m = 66, 67, and 68) ratios. The observed isotope fractionation consists of the mass-dependent and mass-independent isotope effects. The contributions of the nuclear mass and the nuclear volume to the overall isotope effect were evaluated by employing first-principles quantum calculations and using reported isotope shifts in atomic spectra. The magnitude of the mass-dependent isotope effect was explained by the sum of the isotope effect via intramolecular vibrations and the correction to the Born−Oppenheimer electronic energy. The mass-independent isotope effect was correlated with the Gibbs free energy change in the redox reaction.

Introduction

Zinc has five stable isotopes whose natural abundances are 48.63 (^{64}Zn), 27.90 (^{66}Zn), 4.10 (^{67}Zn), 18.75 (^{68}Zn), and 0.62% (^{70}Zn). Isotope separation of ^{64}Zn has an important role for the nuclear power plant. Adding Zn in the primary coolant of boiling water reactors (BWRs) suppresses ^{60}Co buildup (see a review by Lin[1]). Since the highly radioactive isotope ^{65}Zn with the half-life of 245 days is produced by thermal neutron capture by ^{64}Zn, ^{64}Zn-free zinc is desirable for applying this technique. In this context, the isotope separation performance by chemical exchange methods (solvent extraction and liquid chromatography)[2−14] and a centrifugal method[15] has been investigated.

During the past 10 years, stable Zn isotopic variations of natural samples have been extensively studied, with particular interest for biological samples,[16−19] marine samples,[20,21] and extraterrestrial samples.[22−24] Therefore, the mechanisms of isotopic fractionation of Zn attract a lot of interest.

Due to an electropositive potential of the Zn^{2+}/Zn^0 couple, all of the isotope fractionations in aqueous systems[2−14] were attributable to the ligand exchange reactions between Zn(II) complexes. Hence, the isotope fractionation in the redox reaction of the Zn^{2+}/Zn^0 couple is of interest. Isotope fractionation of Zn in an electrochemical reduction has been studied recently, which is a mixture of equilibrium and kinetic systems.[25] Pyrometallurgical biphase extraction, which is a reprocessing technique in nuclear technologies,[26] is a redox equilibrium system at high temperature. In the present study, the isotope effect in a Zn^0−Zn(II) redox reaction is demonstrated with this technique. The isotope effect consists of the mass-dependent and mass-independent isotope fractionations.[27] We verify the contribution of the mass-independent isotope effect by employing the highly precise isotopic analysis, multiple collector ICP mass spectrometry (MC-ICP-MS).

In order to check the validity of the isotope separation factor obtained, we performed the molecular orbital calculations for related zinc complexes. The common calculation methods were chosen, that is, the Hartree−Fock (HF) calculation followed by a Møller−Plesset correlation energy correction truncated at second order (MP2) and density functional theory (DFT).[28] Various basis sets have been used for aqueous complexes of transition metals, for example, Zn, Ni, and Fe,[29−31] and we tested some of them. The equilibrium constant of the isotope exchange reaction was theoretically obtained as the reduced partition function ratio (RPFR) of isotopologues, which has been reported to be effective to estimate the isotope fractionation of Fe.[30,31]

Experimental Section

Pyrometallurgical Biphase Extraction. Zinc metal (99.9999% purity) was a product of Mitsuwa Chemicals Co., Ltd. Anhydrous $CrCl_3$ and alkali chlorides were products of Anderson Physics Laboratory Engineered Materials (99.99% purity). Mole ratios of eutectic mixtures of alkali chlorides used in this study are shown in Table 1. The molten alkali chloride and the liquid zinc were contacted at 923 K in a quartz crucible, and then, 20 mg of $CrCl_3$ was dissolved in the molten salt phase. The contact time was 24 h (6 h is time enough to achieve the equilibrium in a pyrometallurgical biphase extraction[26]). Furthermore, we agitated two phases several times during the extraction in order to avoid the diffusion-controlled effects. The volumes of the two phases at 923 K were 3.2 (molten salt phase)

* To whom correspondence should be addressed. E-mail tosiyuki@rri.kyoto-u.ac.jp. Tel: +81-724-51-2469. Fax: +81-724-51-2634.
† Kyoto University.
‡ Washington University in St. Louis.
§ Tokyo Metropolitan University.
⊥ University of California Davis.
Japan Atomic Energy Agency.

10.1021/jp904882d CCC: $40.75
Published on Web 10/07/2009

TABLE 1: Physical Properties of LiCl and Eutectic Mixtures of Alkali Chlorides

medium	mole ratios	melting point (K)	specific gravity at 923 K (g/mL)	averaged cationic radius[a] (Å)
LiCl		879[b]	1.48−1.49[b]	0.76
LiCl−KCl	[Li]/[K] = 59/41	628[b]	1.542[b]	1.014
LiCl−RbCl	[Li]/[Rb] = 11/9	586[c]	1.93[d]	1.102
LiCl−CsCl	[Li]/[Cs] = 3/2	605[c]	2.23[b]	1.124
NaCl−CsCl	[Na]/[Cs] = 1/2	763[b]	2.47[e]	1.453

[a] Calculated by using mole ratios and ionic radii (six coordinate) in crystals.[32] [b] Literature values.[33] [c] Literature values.[34] [d] Measured in this study by employing the Archimedian method. [e] See ref 35.

TABLE 2: Isotope Fractionation of Zinc

medium	extraction yield (%)	δ^{66}Zn	δ^{67}Zn	δ^{68}Zn
LiCl	0.16	1.03	1.52	2.04
LiCl−KCl	0.22	0.96	1.55	1.97
LiCl−RbCl	0.17	0.95	1.40	1.85
LiCl−CsCl	0.15	1.11	1.61	2.16
NaCl−CsCl	0.14	0.78	1.14	1.54

[a] Internal errors of 2σ are 0.05. External errors of 2σ are 0.10 (δ^{66}Zn), 0.16(δ^{67}Zn), and 0.19(δ^{68}Zn), respectively.

and 1 mL (liquid Zn). Due to the redox potentials of the Cr^{3+}/Cr^0 and Zn^{2+}/Zn^0 couples, the trivalent chromium in the molten salt phase was reduced to be the chromium metal, which was extracted into the metallic zinc phase. The electrically equivalent metallic zinc was oxidized to be the divalent zinc, which was extracted into the molten salt phase (no Zn was found in the molten salt phase without the reductant $CrCl_3$). After achieving the extraction equilibrium, the molten salt phase was drawn into a quartz tube for analysis. The extraction experiment was carried out in a glovebox system filled with dry Ar continuously purified to remove oxygen and humidity. The content of impurities O_2 and H_2O in the inside atmosphere was continuously maintained to less than 1 ppm. The concentrations of Cr and Zn in the drawn salt sample were analyzed by an ICP spectrophotometer (Shimadzu, ICP-1000TR). The extractabilities of Cr were determined to be over 99.3%, suggesting that most of Cr^{3+} in the molten salt phase was reduced to Cr^0 and extracted into the liquid zinc phase (extraction yields of Zn are shown in Table 2). The amount of Zn measured in the drawn salt samples agreed with the electrically equivalent amount.

Isotopic Analysis. Alkali metals and Cr were separated from Zn on anion exchange resin (AG 1−X8, 200−400 mesh) in HBr/HNO_3 as described in refs 22 and 23. The drawn salt sample was dissolved in HBr, dried up by heating once more, and then dissolved into 1.5 M HBr again. On the anion exchange resin in 1.5 M HBr, Zn was strongly adsorbed, while alkali metals and Cr passed through freely. Finally, Zn was collected in 0.5 M HNO_3.

A solution containing 200 ppb Zn in 0.05 M HNO_3 was prepared for isotopic analysis. Isotopic ratios of Zn in all samples were analyzed with the MC-ICP-MS Nu plasma 500 HR at UC Davis coupled with a desolvating nebulizer Nu DSN-100. A total of 40 ratios in 2 blocks of 20 ratios each, with 10 s integration time for each scan, were measured for each sample. The background was corrected for by measuring at half-mass positions from the peak prior to data acquisition. The instrumental mass bias was corrected by bracketing each of the samples with standards. It has been confirmed in the analysis of natural samples that our purification and analytical protocol do not create mass-independent isotope fractionation.[36] The isotope ratios ^{m}Zn/^{64}Zn (m = 66, 67, and 68) were measured. Because of the small abundance of ^{70}Zn (0.62%), this isotope was not used in discussions of the chemical isotope fractionation in our experiments.

Electrochemistry. The formal redox potential of the Zn^{2+}/Zn^0 couple in molten salts was determined by electromotive force (emf) measurements. A liquid zinc electrode was prepared as the working electrode. Zinc metal was placed in a quartz crucible, and then, the temperature was increased over its melting point (692.68 K).[32] A tungsten wire (over 99.95% purity, Nilaco Co. Ltd.) of 1.0 mm diameter was sheathed with a high-purity alumina tube with a 1.0 mm inner diameter and 2.0 mm outer diameter. To create a lead wire, one end of this tube was immersed in the liquid zinc. A silver|silver ion ($Ag|Ag^+$) electrode[35,37] served as the reference electrode. The molten alkali chloride containing 1.00 or 4.85 mol % AgCl was placed in a closed-end Pyrex glass tube, in which a Ag wire of 1.0 mm diameter was immersed. The equilibrium potential between the reference and liquid zinc electrodes was measured at various temperatures (723−1023 K). An electrochemical measurement system Hz-5000 (Hokuto Denko Co. Ltd.) was used for the emf measurement. All procedures were performed in the glovebox system as mentioned above. The potentials determined were converted to the $Cl_2|Cl^-$ standard electrode potentials.[37]

Computational Details. Orbital geometries and vibrational frequencies of Zn(II) chloride complexes were calculated by using the conventional Hartree−Fock (HF) approximation, MP2, and density functional theory (DFT) as implemented by the Gaussian 03 code.[28] The DFT method employed here is a hybrid density functional consisting of Becke's[38] three-parameter nonlocal hybrid exchange potential (B3) with Lee, Yang, and Parr (LYP)[39] nonlocal functionals. The 6-31++G** and 3-21G basis sets were chosen for Li, Na, K, Rb, and Cl, and LanL2DZ[40−43] was chosen for Zn. The former are all-electron basis sets, while the latter is an effective-core potential basis set. For comparison, the 6-311+G** basis set (all-electron basis set) was tested for $ZnCl_4^{2-}$.

As for the mass-independent isotope effect, the contribution of the nuclear volume was estimated by employing all-electron Dirac−Hartree−Fock (DHF) theory, which was implemented in the software package DIRAC08.[44] Calculations of the electronic structure of Zn^0 and Zn^{2+} used Dunning's correction basis sets, cc-pVDZ (double), cc-pVTZ (triple), and cc-pVQZ (quadruple).[45−49]

Results and Discussion

Isotope Fractionation. The pyrometallurgical biphase extraction is a redox reaction system, in which the oxidant Cr(III) reacts as

$$Cr^{3+}(\text{molten salt}) + 3e^- \rightleftarrows Cr^0(\text{liquid Zn}) \qquad (1)$$

and the reductant Zn^0 reacts as

$$Zn^0(\text{liquid Zn}) \rightleftarrows Zn^{2+}(\text{molten salt}) + 2e^- \qquad (2)$$

The extraction equilibrium is

$$2CrCl_3(\text{molten salt}) + 3Zn^0(\text{liquid Zn}) \rightleftarrows 2Cr^0(\text{liquid Zn}) + 3ZnCl_2(\text{molten salt}) \quad (3)$$

In this reaction, the isotope exchange reaction of Zn occurs

$$^{m}ZnCl_2(\text{molten salt}) + {}^{64}Zn^0(\text{liquid Zn}) \rightleftarrows {}^{64}ZnCl_2(\text{molten salt}) + {}^{m}Zn^0(\text{liquid Zn}) \quad (4)$$

The isotope separation factor of Zn between the molten salt and liquid zinc phases, α_m, is defined as

$$\alpha_m = \frac{([^{m}Zn]/[^{64}Zn])_{\text{molten salt}}}{([^{m}Zn]/[^{64}Zn])_{\text{liquid Zn}}} \quad (5)$$

$([^{m}Zn]/[^{64}Zn])_{\text{molten salt}}$ and $([^{m}Zn]/[^{64}Zn])_{\text{liquid zinc}}$ are the isotope ratios of ^{m}Zn relative to ^{64}Zn found in the two phases, respectively. Under the equilibrium state, the number of Zn atoms in the liquid zinc phase is much larger than that in the molten salt phase (see extraction yield of Zn shown in Table 2). Allowing for the isotopic mass balance, $([^{m}Zn]/[^{64}Zn])_{\text{liquid zinc}}$ can be substituted for $([^{m}Zn]/[^{64}Zn])$ of the starting material (Zn metal). The isotope enrichment factor ε_m is defined to be $\varepsilon_m = \alpha_m - 1$. In the present paper, we use δ notation, for which $\delta^{m}Zn$ is defined as

$$\delta^{m}Zn = (\alpha_m - 1) \times 1000 \quad (6)$$

where $\delta^{m}Zn = 1000\varepsilon_m$. Since α_m is close to one, $\alpha_m - 1$ is approximately equal to $\ln \alpha_m$.

The obtained $\delta^{m}Zn$ values are shown in Table 2. The two sigma errors are shown together. A standard deviation of 40 times the isotope ratio measurements per sample was treated as the internal error, while that of six replicates of measuring the same sample was treated as the external error. The errors on $\delta^{m}Zn$ are mainly due to mass spectrometry. In the case of replicate measurements, the mass-dependent bias varies from one run to another, but the isotopic compositions remain strongly correlated. Hence, for the discussion of isotope fractionation in a sample, use of the internal error is appropriate. On the other hand, for the systematic comparison of different samples, using the external error is optimal. The error assessment with a covariance matrix is also effective.[50] As shown in Table 2, for each medium, heavier isotopes were enriched in the molten salt phase. This trend is the same as that found in a redox system by using an electroplating technique.[25] In the redox system by electroplating, $\delta^{66}Zn$=1.7‰ ($Zn(II)/Zn^0$) has been reported.[25] Though experimental conditions are different, our results showed a competitive magnitude, $\delta^{66}Zn = 0.78-1.11$‰.

Mass-Dependent Isotope Effect. The mass-dependent isotope effect originates from the isotopic difference in vibrational energies of isotopologues.[51,52] The isotope enrichment factor ($\sim \ln \alpha_0$) is proportional to $\delta m/mm'$, where δm means the isotopic mass difference of masses m and m' of two isotopes (the prime represents the light isotope). Our experimental system consists of two phases, that is, the liquid zinc and the chloride melt. The intramolecular vibrations of the Zn(II) complex in the molten salt phase should cause the mass-dependent isotope effect.

The structure of the molten $ZnCl_2$ has been studied by Raman spectrometry,[53,54] EXAFS analysis,[55] neutron diffraction analysis,[56] and molecular dynamics calculation.[57] The core structure is considered to be the tetrahedral $ZnCl_4^{2-}$. The possibility of other species such as $ZnCl_3^-$ has been pointed out,[54] but this is inconsistent with the reported coordination number of 4−5.[55−57] Raman spectra have been measured for binary systems, the molten $ZnCl_2$−KCl and $ZnCl_2$−CsCl systems.[58−60] With the increase of the mole ratio of the alkali cation, the polymeric cluster $[ZnCl_4]_n$ changes to the monomeric complex $ZnCl_4^{2-}$ surrounded by the alkali cations.[60] In the present study, the mole ratio of alkali cations is very high (the concentration of Zn^{2+} in the molten salt phase is very small), and hence, the major species of Zn(II) in the chloride melt would be the monomeric $ZnCl_4^{2-}$.

The isotope enrichment factor due to the intramolecular vibrations can be evaluated from the reduced partition function ratio (RPFR), $(s/s')f$, where s is the number of identical configurations obtained by fundamental geometric operations on each molecule such as symmetry or rotation. The $(s/s')f$ is the ratio of the quantum mechanical partition function ratio and the classic partition function ratio.[52] The equation of RPFR is

$$\ln(s/s')f = \sum [\ln b(u_i') - \ln b(u_i)] \quad (7)$$

$$\ln b(u_i) = -\ln u_i + u_i/2 + \ln(1 - e^{-u_i}) \quad (8)$$

$$u_i = h\nu_i/kT \quad (9)$$

whrere h is the Plank constant, k the Boltzmann constant, ν the vibrational frequency, and T the temperature. The subscript i stands for the ith molecular vibrational level, with primed variables referring to the light isotopologue. The isotope enrichment factor due to the molecular vibration can be evaluated from the frequencies (ν) summed over all of the different modes.

The geometry optimization and the vibrational frequency calculation were performed for $ZnCl_4^{2-}$ by employing HF, MP2, and DFT. In a quantum chemical study, the convergence of the reaction energies of the Zn(II) species is excellent in 6-311+G** or higher basis sets.[29] The basis set 6-311+G** was therefore tested for $ZnCl_4^{2-}$. The RPFRs obtained for the isotope pair ^{64}Zn−^{66}Zn at 923 K are shown in Table 3 with the Zn−Cl bond length at the optimized geometry. The RPFRs estimated by HF and DFT showed similar values, while the use of MP2 resulted in ∼10% larger RPFR. The Zn−Cl bond lengths obtained are slightly longer than the value reported for the $ZnCl_2$ melt.[55,56] This may be due to the lack of Zn^{2+} ions surrounding the $ZnCl_4^{2-}$complex in our calculation. The chloride melts used in this study are the mixtures of $ZnCl_2$ and alkali chlorides with small mole fractions of Zn, in which the $ZnCl_4^{2-}$ complex is surrounded by alkali cations. The alkali cations in the secondary sphere of $ZnCl_4^{2-}$ should affect the vibrational modes and frequencies of the $ZnCl_4^{2-}$ complex. Actually, Raman spectrum simulated for $ZnCl_4^{2-}$ did not match with the spectra reported for the molten $ZnCl_2$−KCl and $ZnCl_2$−CsCl mixtures.[59,60] In a quantum chemical study on molten chlorides, the complex with a "linear tetrahedral" structure has been proposed as a stable tetrahedral complex.[61] For example, four alkali cations are set around the tetrahedral $ZnCl_4^{2-}$ with the straight Zn−Cl−alkali

TABLE 3: Reduced Partition Function Ratios and Zn−Cl Bond Lengths of Zn Complexes

species	method, basis[a]	$\ln(s/s')f$[b] ($\times 10^{-3}$)	Zn−Cl bond length[c] (Å)
$ZnCl_4^{2-}$	HF, 6-31++G**	0.254	2.41
$ZnCl_4^{2-}$	MP2, 6-31++G**	0.285	2.37
$ZnCl_4^{2-}$	B3LYP, 6-31++G**	0.251	2.42
$ZnCl_4^{2-}$	B3LYP, 6-311+G**	0.254	2.37
$[Zn(LiCl)_4]^{2+}$	HF, 3-21G	0.307	2.23
$[Zn(NaCl)_4]^{2+}$	HF, 3-21G	0.322	2.38
$[Zn(KCl)_4]^{2+}$	HF, 3-21G	0.329	2.39
$[Zn(RbCl)_4]^{2+}$	HF, 3-21G	0.331	2.39
$[Zn(LiCl)_4]^{2+}$	HF, 6-31++G**	0.269	2.20
$[Zn(NaCl)_4]^{2+}$	HF, 6-31++G**	0.278	2.37
$[Zn(KCl)_4]^{2+}$	HF, 6-31++G**	0.286	2.37

[a] LanL2DZ was used for Zn, except for the case with the 6-311+G** basis set. [b] Calculated for the isotope pair $^{64}Zn-^{66}Zn$ at 923 K. [c] The literature value for the $ZnCl_2$ melt is 2.346 ± 0.010 Å[55] or 2.29 ± 0.02 Å.[56]

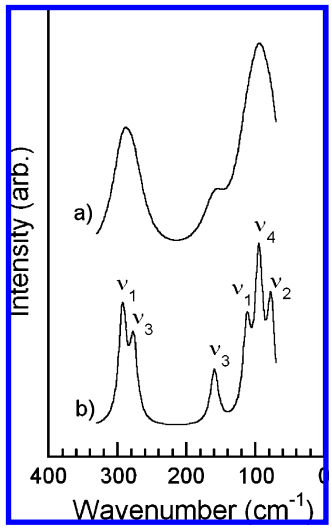

Figure 1. Raman spectra of the $[Zn(KCl)_4]^{2+}$. Spectra are simulated by associating Lorentzian functions to computed wavenumbers. Half-height widths are (a) 20 and (b) 7 cm^{-1}. The quantum chemical calculation was performed by HF with LanL2DZ and 6-31++G**. Vibration modes (ν_1, ν_2, ν_3, and ν_4), which were assigned by referring to our calculation results and a report,[62] are shown together.

alignment. This structure has been reported to correspond to a true minimum on the potential surface.[61] We performed calculations for $[Zn(LiCl)_4]^{2+}$, $[Zn(NaCl)_4]^{2+}$, $[Zn(KCl)_4]^{2+}$, and $[Zn(RbCl)_4]^{2+}$. Raman spectra simulated for $[Zn(KCl)_4]^{2+}$ are shown in Figure 1 as an example. Figure 1a is similar to the Raman spectra of the molten $ZnCl_2-KCl$ and $ZnCl_2-CsCl$ mixtures,[59,60] and Figure 1b is similar to the Raman spectrum of the solid $ZnCl_2-CsCl$ mixture.[60] According to our calculations, $\delta^{66}Zn \sim 0.3$ can be expected as the mass effect via intramolecular vibrations. $\delta^{66}Zn$ (Table 2) and the RPFRs (Table 3) are shown together in Figure 2. The mass effects observed are twice as large or more than those expected by our quantum chemical calculations.

To check the validity of the RPFRs in Table 3, the RPFR was also calculated by using the reported vibrational frequency measured for the molten $ZnCl_2-KCl$ and $ZnCl_2-CsCl$ systems. The RPFR derived by the Bigeleisen−Mayer approximation[52] can be simplified as

$$\ln(s/s')f = \frac{\delta mnMu^2}{24mm'} \quad (10)$$

where n is the number of ligands with the mass M ($n = 4$ and $M = 35.45$ for $ZnCl_4^{2-}$). $\delta^{66}Zn$ deals with $m' = 64$, $m = 66$, and $\delta m = m - m' = 2$. The u can be calculated from the frequency of totally symmetric vibration (ν_1) and temperature (eq 9). The molten $ZnCl_2-KCl$ system shows $\nu_1 = 278$ cm^{-1},[59] while the molten $ZnCl_2-CsCl$ system shows $\nu_1 = 277$ cm^{-1}.[60] The spectral resolution has been reported to be 1.2 cm^{-1}.[58] By substituting the averaged value (277.5 cm^{-1}) into eq 10, the RPFR at 923 K was calculated to be 0.527‰. If the RPFR of Zn^0 is set to be zero, $\ln(s/s')f$ in eq 10 can be treated as the conventional mass-dependent isotope effect ($\ln \alpha_0$), and this value may be comparable with $\delta^{66}Zn$. This value is shown in Figure 4 as the dotted line (i). The RPFR calculated by eq 10 showed a midvalue between our experimental results and quantum chemical calculations.

The RPFR calculated by eq 10 is still smaller than the mass effects observed. This suggests that the other mass effects should exist. The correction term, $\ln K_{BOELE}$, to the Born−Oppenheimer approximation has been reported as another mass-dependent isotope effect.[27,63−65] The Born−Oppenheimer approximation stands on the assumption that isotopologues have identical electronic energies. On this basis, only the mass effect via intramolecular vibrations occurs upon identical potential surfaces. Since the nucleus is much heavier than an electron, it moves relatively slowly and may be considered as stationary. For light nuclides, however, the movement of the nucleus can no longer be neglected, and its movement around the center of gravity of the nucleus−electrons ensemble creates a kinetic momentum. Each orbital electron receives an excess kinetic momentum via the movement of the nucleus, which is a function of the mass. The excess momenta cause the mass-dependent isotope effect, $\ln K_{BOELE}$. The correction to the Born−Oppenheimer electronic energy ($\ln K_{BOELE}$) has been calculated in the pioneering study on lighter diatomic isotopomers.[63−65] Although the parameters for calculating $\ln K_{BOELE}$ are not available for zinc, its magnitude is presumed from the mass shift found in atomic spectra. The excess momenta mentioned

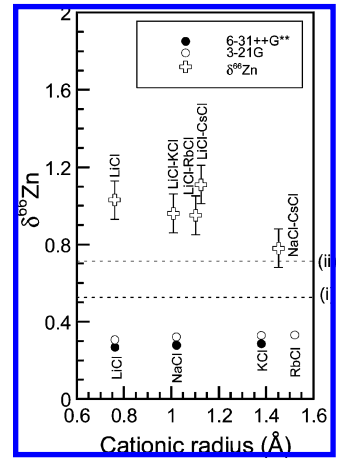

Figure 2. Mass effect contribution to $\delta^{66}Zn$ versus the averaged cationic radius. $\delta^{66}Zn$ (see Table 2) are shown with the external error $2\sigma = 0.10$. The mass effects via intramolecular vibrations calculated (see Table 3) are shown together. The dotted line (i) shows the $\ln \alpha_0$ value calculated by the classic theory with the Bigeleisen−Mayer approximation.[52] The dotted line (ii) shows the sum of $\ln \alpha_0 + \ln K_{BOELE}$, in which $\ln K_{BOELE}$ was estimated from the mass shift found in an ss−pd transition.[67]

TABLE 4: Reported Mass Shifts and Nuclear Field Shifts for $^{64}Zn-^{66}Zn$

valence	Zn(I)[c]	Zn(I)[d]	Zn[0][e]
transition	$3d^{10}4p\ ^2P_{1/2}-3d^9 4s^2\ ^2D_{3/2}$	$4s\ ^2S_{1/2}-4p\ ^2P_{3/2}$	$4s^2\ ^1S_0-4s4p\ ^3P_1$
transition energy (nm)	589.4	202	307.6
mass shift, δE_{ms}[a] (GHz)	3.58 ± 0.15	1.03	0.921 ± 0.031
field shift, δE_{fs}[a] (GHz)	0.735	0.35	
$\delta E_{ms}/kT$[b] ($\times 10^{-3}$)	0.186	0.054	0.048
$\delta E_{fs}/kT$[b] ($\times 10^{-3}$)	0.038	0.018	

[a] Absolute values. [b] $T = 923$ K. [c] Reference 67. [d] Reference 68. The error of the measured isotope shift has been reported to be 0.006 GHz. [e] Reference 69.

above shift the atomic energy levels. This results in an isotope shift in atomic spectra called the mass shift.[66] Zinc isotopes are known to have quite large mass shifts.[66−69] The reported isotope shifts are summarized in Table 4 along with reported errors. The electronic transition, in which a 3d-orbital electron participates, gives a larger mass shift compared with that in the 4s−4p transitions.

The electronic partition function, Q_e, can be written as

$$Q_e = \exp(-\delta E_e/kT) \tag{11}$$

where δE_e means the isotopic difference in the related molecular energy level. The contributions of the mass shift to Q_e and δE_e are written as Q_{ms} and δE_{ms}. K_{BOELE} in our system is

$$K_{BOELE} = \frac{(Q_{ms})_{molten\ salt}}{(Q_{ms})_{liquid\ Zn}} = \frac{\exp(-\delta E_{ms}/kT)_{molten\ salt}}{\exp(-\delta E_{ms}/kT)_{liquid\ Zn}} \tag{12}$$

Hence, ln K_{BOELE} is

$$\ln K_{BOELE} = \frac{(\delta E_{ms})_{liquid\ Zn} - (\delta E_{ms})_{molten\ salt}}{kT} \tag{13}$$

The apparent electron configuration of Zn^0 in the liquid Zn phase may be $3d^{10}4s^2$, in which 4s electrons act as free electrons. Theoretical and experimental studies on the electronic structure of Zn metal showed that the position of the 3d bands lies within the conduction band.[70,71] This suggests that the cohesion of Zn metal is affected by the 3d electrons. A theoretical study on the cohesive energy of Zn group metals also indicates that the repulsive effect of the filled d shell on the valence s electrons occurrs.[72,73] The tetrahedral $ZnCl_4^{2-}$ complex possesses the sp^3 hybrid orbital. This hybrid orbital might be interfered by the 3d electrons because an interaction between p and d orbitals has been pointed out for Zn complexes.[74] Consequently, it is considered that the 3d electrons participate in the redox reaction in our system. As a maximum value, ln $K_{BOELE} \sim 0.186$‰ (see Table 4) therefore can be expected. The dotted line (ii) shown in Figure 2 is the sum of ln α_0 (0.527‰) and ln K_{BOELE} (0.186‰). The dotted line (ii) matches the mass effect found in the NaCl−CsCl system.

Although the mass effect found in the NaCl−CsCl system is possible, other results deviate from the expected value. The deviation seems to increase with the decrease of the averaged cationic radius. This should result from differences in physicochemical properties of the chloride melts because the liquid Zn phase is identical for all experiments. The specific conductance (923 K) per molarity of alkali cations is shown in Figure 3, which increases with the decrease of the averaged cationic radius. A medium with larger specific conductance per unit molarity would possess more conducting electrons, and/or the conducting electrons would have larger mobility. The large mobility of electrons suggests the large momenta of them. Hence, the larger specific conductance per unit molarity may be correlated with an increase of ln K_{BOELE}.

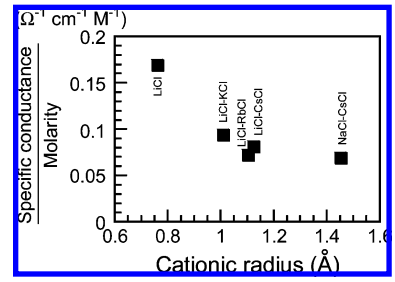

Figure 3. Specific conductivity per molarity versus cationic radius. Specific conductance data at 923 K are literature values.[33] Molarities were calculated from the data shown in Table 1.

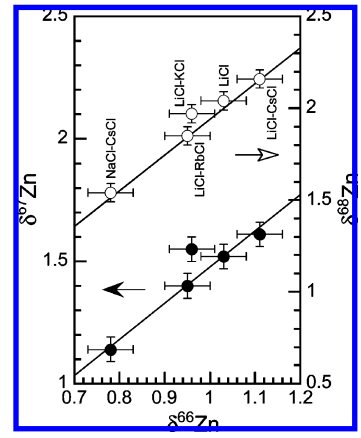

Figure 4. Correlation of δ^mZn values. The δ^mZn values shown in Table 2 are shown with the internal error $2\sigma = 0.05$. The straight lines are $\delta^{67}Zn = 1.478 \times \delta^{66}Zn$ and $\delta^{68}Zn = 1.941 \times \delta^{66}Zn$, where the slopes were calculated from the relation of $\delta m/m'$.

Mass-Independent Isotope Effect. The correlations of the δ^mZn values (see Table 2) are shown in Figure 4. The mass-dependent lines are shown together. δ^mZn showed a mass-dependent trend, but a breakdown can be seen for the LiCl−KCl system. This suggests that the mass-independent isotope fractionation occurred in this system.

The classic theory of chemical isotope fractionation is based on the mass-dependent isotope effect via the isotopic difference in vibrational energies of isotopologues.[51,52] The original theory has been extended to include some correction terms.[27]

$$\ln \alpha = \ln \alpha_0 + \ln K_{BOELE} + \ln K_{fs} + \ln K_{hf} \tag{14}$$

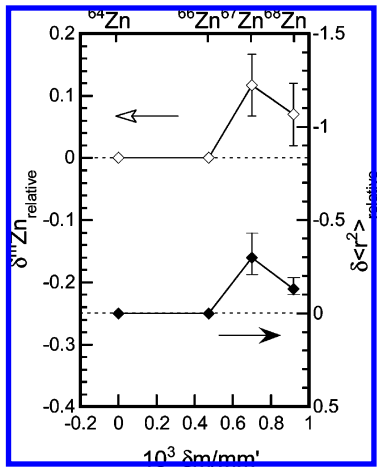

Figure 5. Normalized δ^mZn and $\delta\langle r^2\rangle$ as functions of $\delta m/mm'$. The δ^mZn values of the LiCl−KCl system and the reported relative $\delta\langle r^2\rangle$ values[67] are normalized for an isotope pair ^{64}Zn−^{66}Zn by using the exponential law.[77] The 2σ internal errors are drawn for δ^{67}Zn and δ^{68}Zn. The reported errors[67] of $\delta\langle r^2\rangle$ are also shown. The dotted lines are baselines.

where ln K_{fs} is the nuclear field shift term and ln K_{hf} is the term of the nuclear spin. ln K_{hf} has been treated as a minor correction term, while ln K_{fs} has been treadted as the major correction term corresponding to the mass-independent isotope effect.[27]

The nuclear field shift effect is recognized as the origin of the mass-independent isotope fractionation in chemical exchange reactions.[27,75] The nuclear field shift is an isotope shift in orbital electrons.[66] This results from the isotopic difference in the nuclear size and shape. Different isotopes have the same number of protons, but they do not have the same distribution of protons in space. That is, the nuclear charge distribution, which is usually represented as the mean-square charge radius $\langle r^2\rangle$, is affected by the number of neutrons in the nucleus. The nuclear charge distribution gives an electric field, and its isotopic difference shifts the atomic energy levels, also displacing the electronic molecular states. The nuclear field shift is not mass-dependent but is strongly related to the neutron configuration of nuclear structure. The nuclear field shift effect is thus the mass-independent isotope effect. In general, the field shift is smaller than the mass shift for light elements, but for heavy elements, the field shift is relatively large compared to the mass shift (see Figure 1 in ref 76).

In order to check the relation between δ^mZn and $\delta\langle r^2\rangle$, we subtract the linear component from δ^mZn's of the LiCl−KCl system by employing the exponential law.[77] This normalization is effective to see the mass-independent component of Cd, which is a congener of Zn.[78] The result is shown in Figure 5. The normalized δ^mZn versus $\delta m/mm'$ possesses the similar profile of the normalized $\delta\langle r^2\rangle$ versus $\delta m/mm'$. This strongly supports the existence of the nuclear field shift effect in the Zn isotope fractionation.

At a constant temperature, eq 14 can be simplified as

$$\ln \alpha = \delta\langle r^2\rangle A + \frac{\delta m}{mm'}B \qquad (15)$$

where A and B are scaling factors for the nuclear field shift effect and the mass effect, respectively.[79] The contributions of the mass effect and the nuclear field shift effect were separated by the same manner as that reported in our previous studies.[5,6,78,79]

TABLE 5: Nuclear Field Shift Effect and Mass Effect[a]

(a) $\delta\langle r^2\rangle$ and $\delta m/mm'$

m	$\delta\langle r^2\rangle$[b]/relative value	$\delta m/mm'/10^{-3}$
64	0	0
66	1.00	0.473
67	1.19	0.700
68	1.84	0.919

(b) LiCl−KCl System

m	δ^mZn/‰	nuclear field shift effect/‰	mass effect/‰	nuclear field shift effect + mass effect/‰
64	0	0	0	0
66	0.96	−0.34	1.33	0.99
67	1.55	−0.41	1.96	1.56
68	1.97	−0.63	2.58	1.95

[a] Scaling factors A and B in eq 15 were calculated to be −0.3407 and 2805, respectively, with the determination coefficient R^2 = 0.99994. [b] Literature values.[67]

The results are shown in Table 5. The sum values in Table 5 show quite good agreement with δ^mZn experimentally obtained.

Recent quantum chemical studies have adopted finite nucleus models into ab initio methods.[80−82] The validity of the magnitude of the nuclear field shift effect has been confirmed for Hg, Tl, and U redox reactions. In the present study, the total electronic energies at the ground states of Zn^0 and Zn^{2+} were calculated for different isotopes with different nuclear charge radii. A relativistic method was applied, the Dirac−Coulomb Hartree−Fock (DCHF) method.[44] A relativistic method, in which an approximation[83] was used, was also tested. The nonrelativistic (NR) method was performed for comparison. The theoretical background and computational details can be seen elsewhere.[44,80−82] The root-mean-square radii ($\langle r^2\rangle^{1/2}$) reported in the literature (^{64}Zn: 3.9286 fm; ^{66}Zn: 3.9496 fm)[84] were used in the calculation. The calculation results for ^{64}Zn and ^{66}Zn are shown in Table 6 in atomic units (au).

Similar to eqs 11−13, the nuclear field shift effect, ln K_{fs}, can be written as

$$\ln K_{fs} = \frac{(\delta E_{fs})_{\text{liquid Zn}} - (\delta E_{fs})_{\text{molten salt}}}{kT} \qquad (16)$$

As a first approximation, δE_{fs}'s for Zn^0 and Zn^{2+} were substituted into $(\delta E_{fs})_{\text{liquid zinc}}$ and $(\delta E_{fs})_{\text{molten salt}}$, respectively. ln K_{fs} at 923 K was estimated to be 0.011−0.013‰ (Table 6). In our calculation, using the relativistic method resulted in a smaller ln K_{fs}, while using the larger basis set gave a larger ln K_{fs}; nevertheless, the differences are marginal. It is of interest that the value estimated is close to the $\delta E_{fs}/kT$ value (=0.018‰; see Table 4) calculated from the field shift found in the 4s−4p transition.[68] Theoretically and experimentally, the isotopic differences between the electronic energy levels with and without the 4s orbital are consistent with each other. As we mentioned above, 3d electrons are considered to participate in our redox system, and therefore, ln K_{fs} ~0.038‰ (see Table 4) may be expected.

The nuclear field shift effect found in the LiCl−KCl system is larger than our anticipated magnitude. The result suggests that the probability density of electrons in the Zn nucleus may be unusual in the LiCl−KCl system. If the electron configuration of $ZnCl_4^{2-}$ in this melt is unusual, the complex should be unstable. In order to verify the stability of the $ZnCl_4^{2-}$ complex

TABLE 6: Total Energy of Zn(II) and Zn^0 for Isotopes ^{64}Zn and ^{66}Zn

method[a]	basis set	Zn^{2+} total energy (au), ^{64}Zn, ^{66}Zn	Zn^0 total energy (au), ^{64}Zn, ^{66}Zn	ln K_{fs}[b] ($\times 10^{-3}$)
DCHF	cc-pVDZ	−1792.9544921898, −1792.9544248868	−1793.8580741774, −1793.8580068404	0.0116
LVCORR	cc-pVDZ	−1792.9621835218, −1792.9621162186	−1793.8657719769, −1793.8657046399	0.0116
NR	cc-pVDZ	−1776.9511543886, −1776.9510863941	−1777.8404076675, −1777.8403396367	0.0116
DCHF	cc-pVTZ	−1792.9672631768, −1792.9671958282	−1793.8718994742, −1793.8718320905	0.0120
LVCORR	cc-pVTZ	−1792.9749783243, −1792.9749109757	−1793.8796222069, −1793.8795548231	0.0120
NR	cc-pVTZ	−1776.9512661079, −1776.9511981144	−1777.8404095569, −1777.8403415259	0.0128
DCHF	cc-pVQZ	−1792.9858662368, −1792.9857984847	−1793.8905827833, −1793.8905149949	0.0124
LVCORR	cc-pVQZ	−1792.9936102767, −1792.9935425244	−1793.8983345620, −1793.8982667734	0.0124
NR	cc-pVQZ	−1776.9526370927, −1776.9525689275	−1777.8416684967, −1777.8416002940	0.0129

[a] DCHF: Dirac−Coulomb Hartree−Fock method. LVCORR: Relativistic method including L. Visscher's correction.[83] NR: Nonrelativistic method. [b] $T = 923$ K.

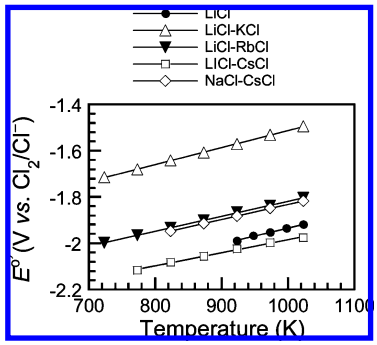

Figure 6. Temperature dependence of the redox potential of the Zn^{2+}/Zn^0 couple. Temperature ranges are 723−1023 (LiCl−KCl, LiCl−RbCl, and LiCl−CsCl), 823−1023 (NaCl−CsCl), and 923−1023 K (LiCl). The lower temperature limits were set by considering their melting points (see Table 1).

TABLE 7: Formal Redox Potential of the Zn^{2+}/Zn^0 Couple ($E^{\circ\prime} = A + BT$)

medium	A (V)	B (10^{-4}V/K)	determination coefficient	ΔG° at 923 K[a] (kJ/mol)
LiCl	−2.626	6.920	0.998	383.8
LiCl−KCl	−2.249	7.364	>0.999	303.4
LiCl−RbCl	−2.466	6.470	>0.999	360.3
LiCl−CsCl	−2.551	5.662	0.997	390.8
NaCl−CsCl	−2.481	6.490	>0.999	363.1

[a] Experimentally obtained in the present study; 2σ errors were estimated to be 1.9 kJ/mol.

in chloride melts, the formal redox potential (apparent) of the Zn^{2+}/Zn^0 couple, $E^{\circ\prime}$, was measured. The results obtained were shown in Figure 6 and Table 7. The temperature dependence of $E^{\circ\prime}$ was precisely determined with determination coefficients of 0.997 or better (Table 7). Note that the LiCl−KCl system gives the largest intercept and slope in all systems (Figure 6). Since the liquid Zn phase is identical for all experiments, the large $E^{\circ\prime}$ means instability of the Zn(II) complex, that is, $ZnCl_4^{2-}$. The larger slope means that the $ZnCl_4^{2-}$ complex destabilizes more with the increase of temperature. The Gibbs free energy change, ΔG°, can be calculated as $-nFE^{\circ\prime}$, where n means the number of electrons exchanged in the redox reaction and F the Faraday constant. The ΔG° values at 923 K were shown in Table 7. ΔG° found in the LiCl−KCl system is 50 kJ/mol or smaller than that found in other systems. The smallest ΔG° means that the $ZnCl_4^{2-}$ is most instable in this melt. The electron density at the Zn nucleus may be unusually large in the LiCl−KCl eutectic melt, which may be correlated with the instability of the $ZnCl_4^{2-}$ complex. It should be noted that an alternative origin of the mass-independent isotope fractionation might be the magnetic isotope effect, but this is the effect found in kinetic systems (see section 5 in a review in ref 79). Hence, the nuclear field shift effect is the most possible origin for our equilibrium system.

Conclusions

Zinc isotopes were fractionated in the Zn^0−Zn(II) redox reaction. The mass-dependent isotope effect observed could be identified to be the conventional mass effect via intramolecular vibrations and the correction to the Born−Oppenheimer electronic energy. The isotope fractionation observed in the LiCl−KCl system consisted of the mass effects and the nuclear field shift effect. The nuclear field shift effect would be correlated with the instability of the related Zn complex.

Acknowledgment. The authors thank two anonymous reviewers for useful suggestions and constructive comments on the manuscript. T.F. thanks Roy Jacobus for his help in improving the English of this paper. Q.-Z.Y. acknowledges support from NASA's Cosmochemistry Program (NNX08AG-57G) and Origins of Solar Systems Program (NNX09AC93G) for some aspects of the work described in this paper. This is a UCD-ICP-MS contribution number #0024. F.M. acknowledges support from NASA-Laser program (NNX09AM64G).

References and Notes

(1) Lin, C. C. *Prog. Nucl. Energy* **2009**, *51*, 207.
(2) Nishizawa, K.; Nakamura, K.; Yamamoto, T.; Masuda, T. *Solvent Extr. Ion Exch.* **1993**, *11*, 389.
(3) Nishizawa, K.; Satoyama, T.; Miki, T.; Yamamoto, T.; Nomura, M. *Sep. Sci. Technol.* **1996**, *31*, 2831.
(4) Nishizawa, K.; Miki, T.; Satoyama, T.; Fujii, T.; Yamamoto, T.; Nomura, M. *Sep. Sci. Technol.* **1998**, *33*, 991.
(5) Nishizawa, K.; Maeda, Y.; Kawashiro, F.; Fujii, T.; Yamamoto, T.; Hirata, T. *Sep. Sci. Technol.* **1998**, *33*, 2101.
(6) Fujii, T.; Hirata, T.; Shibahara, Y.; Nishizawa, K. *Phys. Chem. Chem. Phys.* **2001**, *3*, 3125.
(7) Ban, Y.; Nomura, M.; Fujii, Y. *J. Nucl. Sci. Technol.* **2002**, *39*, 156.
(8) Ding, X. C.; Nomura, M.; Suzuki, T.; Sugiyama, Y.; Kaneshiki, T.; Fujii, Y. *J. Chromatogr., A* **2006**, *1113*, 182.
(9) Ding, X. C.; Syzuki, T.; Nomura, M.; Sugiyama, Y.; Kaneshiki, T.; Fujii, Y. *Bull. Chem. Soc. Jpn.* **2006**, *79*, 1389.
(10) Ding, X. C.; Kim, H.-J.; Nomura, M.; Suzuki, T.; Sugiyama, Y.; Fujii, Y. *J. Nucl. Sci. Technol.* **2006**, *43*, 411.
(11) Zhang, Y.-H.; Fukuda, Y.; Nomura, M.; Fujii, Y.; Oi, T. *J. Nucl. Sci. Technol.* **2006**, *43*, 415.
(12) Fukuda, Y.; Zhang, Y.-H.; Suzuki, T.; Fujii, Y.; Oi, T. *J. Nucl. Sci. Technol.* **2006**, *43*, 446.
(13) Ding, X. C.; Suzuki, T.; Nomura, M.; Kim, H.-J.; Sugiyama, Y.; Fujii, Y. *J. Radioanal. Nucl. Chem* **2007**, *273*, 79.
(14) Tan, Y.; Kan, D.; Ding, X.; Nomura, M.; Fujii, Y. *J. Nucl. Sci. Technol.* **2008**, *45*, 1078.
(15) Tcheltsov, A. N.; Sosnin, L. Yu.; Shipilov, Yu. D.; Zaozersky, Yu. P.; Khamylov, V. K.; Pochekutov, T. S. *Nucl. Instrum. Methods Phys. Res., Sect. A* **2006**, *561*, 52.
(16) Moynier, F.; Pichat, S.; Pons, M.-L.; Fike, D.; Balter, V.; Albarède, F. *Chem. Geol.* **2009**, *267*, 125.

(17) Weiss, D. J.; Mason, T. F. D.; Zhao, F. J.; Kirk, G. J. D.; Coles, B. J.; Horstwood, M. S. A. *New Phytol.* **2005**, *165*, 703.
(18) Viers, J.; Oliva, P.; Nonell, A.; Gélabert, A.; Sonke, J. E.; Freydier, R.; Gainville, R.; Dupré, B. *Chem. Geol.* **2007**, *239*, 124.
(19) John, S. G.; Geis, R. W.; Saito, M. A.; Boyle, E. A. *Limnol. Oceanogr.* **2007**, *52*, 2710.
(20) Pichat, S.; Douchet, C.; Albarède, F. *Earth Planet. Sci.* **2003**, *210*, 167.
(21) Gélabert, A.; Pokrovsly, O. S.; Viers, J.; Schott, J.; Boudou, A.; Feurtet-Mazel, A. *Geochim. Cosmochim. Acta* **2006**, *70*, 839.
(22) Moynier, F.; Blichert-Toft, J.; Telouk, P.; Luck, J.-M. *Geochim. Cosmochim. Acta* **2007**, *71*, 4365.
(23) Moynier, F.; Albarède, F.; Herzog, G. F. *Geochim. Cosmochim. Acta* **2006**, *70*, 6103.
(24) Luck, J.-M.; Othman, D. B.; Albarède, F. *Geochim. Cosmochim. Acta* **2005**, *69*, 5351.
(25) Kavner, A.; John, S. G.; Sass, S.; Boyle, E. A. *Geochim. Cosmochim. Acta* **2008**, *72*, 1731.
(26) Yamana, H.; Wakayama, N.; Souda, N.; Moriyama, H. *J. Nucl. Mater.* **2000**, *278*, 37–47.
(27) Bigeleisen, J. *J. Am. Chem. Soc.* **1996**, *118*, 3676.
(28) Frisch, M. J.; Trucks, G. W.; Schlegel, H. B.; Scuseria, G. E.; Robb, M. A.; Cheeseman, J. R.; Montgomery, J. A., Jr.; Vreven, T.; Kudin, K. N.; Burant, J. C.; Millam, J. M.; Iyengar, S. S.; Tomasi, J.; Barone, V.; Mennucci, B.; Cossi, M.; Scalmani, G.; Rega, N.; Petersson, G. A.; Nakatsuji, H.; Hada, M.; Ehara, M.; Toyota, K.; Fukuda, R.; Hasegawa, J.; Ishida, M.; Nakajima, T.; Honda, Y.; Kitao, O.; Nakai, H.; Klene, M.; Li, X.; Knox, J. E.; Hratchian, H. P.; Cross, J. B.; Bakken, V.; Adamo, C.; Jaramillo, J.; Gomperts, R.; Stratmann, R. E.; Yazyev, O.; Austin, A. J.; Cammi, R.; Pomelli, C.; Ochterski, J. W.; Ayala, P. Y.; Morokuma, K.; Voth, G. A.; Salvador, P.; Dannenberg, J. J.; Zakrzewski, V. G.; Dapprich, S.; Daniels, A. D.; Strain, M. C.; Farkas, O.; Malick, D. K.; Rabuck, A. D.; Raghavachari, K.; Foresman, J. B.; Ortiz, J. V.; Cui, Q.; Baboul, A. G.; Clifford, S.; Cioslowski, J.; Stefanov, B. B.; Liu, G.; Liashenko, A.; Piskorz, P.; Komaromi, I.; Martin, R. L.; Fox, D. J.; Keith, T.; Al-Laham, M. A.; Peng, C. Y.; Nanayakkara, A.; Challacombe, M.; Gill, P. M. W.; Johnson, B.; Chen, W.; Wong, M. W.; Gonzalez, C.; Pople, J. A. *Gaussian 03*, revision B.05; Gaussian, Inc.: Pittsburgh, PA, 2003.
(29) Rulíšek, L.; Havlas, Z. *J. Phys. Chem. A* **1999**, *103*, 1634.
(30) Hill, P. S.; Schauble, E. A. *Geochim. Cosmochim. Acta* **2008**, *72*, 1939.
(31) Fujii, T.; Moynier, F.; Telouk, P.; Albarède, F. Z. *J. Phys. Chem. A* **2006**, *110*, 11108.
(32) Lide, D. R., Ed. *CRC Handbook of Chemistry and Physics*, 89th ed.; CRC Press: Boca Raton, FL, 2008.
(33) Janz, G. J.; Tomkins, R. P. T.; Allen, C. B.; Downey, J. R., Jr.; Gardner, G. L.; Krebs, U.; Singer, S. K. *J. Phys. Chem. Ref. Data* **1975**, *4*, 871.
(34) Cook, L. P., McMurdie, H. F., Eds. *Phase Diagrams for Ceramists, Volume VII, Salts*; The American Ceramic Society: OH, 1989.
(35) Nagai, T.; Fujii, T.; Shirai, O.; Yamana, H. *J. Nucl. Sci. Technol.* **2004**, *41*, 690.
(36) Moynier, F.; Dauphas, N.; Podosek, F. A. *Astrophys. J.* **2009**, *700*, L92.
(37) Shirai, O.; Nagai, T.; Uehara, A.; Yamana, H. *J. Alloys Compd.* **2008**, *456*, 498.
(38) Becke, A. D. *J. Chem. Phys.* **1993**, *98*, 5648.
(39) Lee, C. T.; Yang, W. T.; Parr, R. G. *Phys. Rev. B* **1988**, *37*, 785.
(40) Dunning, T. H.; Hay, P. J. In *Modern Theoretical Chemistry*, Schaefer, H. F., Ed.; Plenum: New York, 1976; Vol. 3, p 1.
(41) Hay, P. J.; Wadt, W. R. *J. Chem. Phys.* **1985**, *82*, 270.
(42) Wadt, W. R.; Hay, P. J. *J. Chem. Phys.* **1985**, *82*, 284.
(43) Hay, P. J.; Wadt, W. R. *J. Chem. Phys.* **1985**, *82*, 299.
(44) Visscher, L.; Jensen, H. J. Aa.; Saue, T. Dirac, a relativistic ab initio electronic structure program, with new contributions from Bast, R.; Dubillard, S.; Dyall, K. G.; Ekström, U.; Eliav, E.; Fleig, T.; Gomes, A. S. P.; Helgaker, T. U.; Henriksson, J.; Ilias, M.; Jacob, Ch. R.; Knecht, S.; Norman, P.; Olsen, J.; Pernpointner, M.; Ruud, K.; Salek, P.; Sikkema, J. *DIRAC08*, Release 0; http://dirac.chem.sdu.dk (2008).
(45) Woon, D. E.; Dunning, T. H., Jr. *J. Chem. Phys.* **1993**, *98*, 1358.
(46) Kendall, R. A.; Dunning, T. H., Jr.; Harrison, R. J. *J. Chem. Phys.* **1992**, *96*, 6796.
(47) Dunning, T. H., Jr. *J. Chem. Phys.* **1989**, *90*, 1007.
(48) Peterson, K. A.; Woon, D. E.; Dunning, T. H., Jr. *J. Chem. Phys.* **1994**, *100*, 7410.
(49) Wilson, A.; van Mourik, T.; Dunning, T. H., Jr. *J. Mol. Struct: THEOCHEM* **1997**, *388*, 339.
(50) Fujii, T.; Moynier, F.; Telouk, P.; Albarède, F. *Astrophys. J.* **2006**, *647*, 1506.
(51) Urey, H. C. *J. Chem. Soc.* **1947**, 562.
(52) Bigeleisen, J.; Mayer, M. G. *J. Chem. Phys.* **1947**, *15*, 261.
(53) Irish, D. E.; Young, T. F. *J. Chem. Phys.* **1965**, *43*, 1765.
(54) Ellis, R. B. *J. Electrochem. Soc.* **1966**, *113*, 485.
(55) Wong, J.; Lytle, F. W. *J. Non-Cryst. Solids* **1980**, *37*, 273.
(56) Biggin, S.; Enderby, J. E. *J. Phys. C* **1981**, *14*, 3129.
(57) Woodcock, L. V.; Angell, C. E.; Cheeseman, P. *J. Chem. Phys.* **1976**, *65*, 1565.
(58) Moyer, J. R.; Evans, J. C.; Lo, G. Y.-S. *J. Electrochem. Soc.* **1966**, *113*, 158.
(59) Itoh, M.; Sakai, K.; Nakamura, T. *Inorg. Chem.* **1982**, *21*, 3552.
(60) Begun, G. M.; Brynestad, J.; Fung, K. W.; Mamantov, G. *Inorg. Nucl. Chem. Lett.* **1972**, *8*, 79.
(61) Hezebroucq, S.; Picard, G. S.; Adamo, C. *J. Chem. Phys.* **2005**, *122*, 224512.
(62) Quicksall, C. O.; Spiro, T. G. *Inorg. Chem.* **1966**, *5*, 2232.
(63) Kleinman, L. I.; Wolfsberg, M. *J. Chem. Phys.* **1973**, *59*, 2043.
(64) Kleinman, L. I.; Wolfsberg, M. *J. Chem. Phys.* **1974**, *60*, 4740.
(65) Kleinman, L. I.; Wolfsberg, M. *J. Chem. Phys.* **1974**, *60*, 4749.
(66) King, W. H. *Isotope Shifts in Atomic Spectra*; Plenum Press: New York, 1984.
(67) Foot, C. J.; Stacy, D. N.; Stacy, V.; Kloch, R.; Leś, Z. *Proc. R. Soc. London, Ser. A* **1982**, *384*, 205.
(68) Matsubara, K.; Tanaka, U.; Imajo, H.; Urabe, S.; Watanabe, M. *Appl. Phys. B: Laser Opt.* **2003**, *76*, 209.
(69) Campbell, P.; Billowes, J.; Grant, I. S. *J. Phys. B* **1997**, *30*, 2351.
(70) Juras, G. E.; Segall, B.; Sommers, C. B. *Solid State Commun.* **1972**, *10*, 427.
(71) Himpsel, F. J.; Eastman, D. E.; Koch, E. E.; Williams, A. R. *Phys. Rev. B* **1980**, *22*, 4604.
(72) Chelikowsky, J. R. *Phys. Rev. Lett.* **1981**, *47*, 387.
(73) Alonso, J. A.; March, N. H. *Electrons in Metals and Alloys*; Academic Press: London, 1989.
(74) Schröer, P.; Krüger, P.; Pollmann, J. *Phys. Rev. B* **1993**, *47*, 6971.
(75) Nomura, M.; Higuchi, N.; Fujii, Y. *J. Am. Chem. Soc.* **1996**, *118*, 9127.
(76) Stern, R. C.; Snavely, B. B. *Ann. N.Y. Acad. Sci.* **1976**, *267*, 71.
(77) Albarède, F.; Telouk, P.; Blichert-Toft, J.; Boyet, M.; Agranier, A.; Nelson, B. *Geochim. Cosmochim. Acta* **2004**, *68*, 2715.
(78) Fujii, T.; Moynier, F.; Telouk, P.; Albarède, F. *Chem. Geol.* **2009**, *267*, 157.
(79) Fujii, T.; Moynier, F.; Albarède, F. *Chem. Geol.* **2009**, *267*, 139.
(80) Schauble, E. A. *Geochim. Cosmochim. Acta* **2007**, *71*, 2170.
(81) Abe, M.; Suzuki, T.; Fuji, Y.; Hada, M. *J. Chem. Phys.* **2008**, *128*, 144309.
(82) Abe, M.; Suzuki, T.; Fujii, Y.; Hada, M.; Hirao, K. *J. Chem. Phys.* **2008**, *129*, 164309.
(83) Visscher, L. *Theor. Chem. Acc.* **1997**, *98*, 68.
(84) Angeli, I. *At. Data Nucl. Data Tables* **2004**, *87*, 185.

JP904882D